coatings

MDPI

Article

Influence of N_2 Gas Flow Ratio and Working Pressure on Amorphous Mo–Si–N Coating during Magnetron Sputtering

Ki Seong Lim [1], Young Seok Kim [1], Sung Hwan Hong [1], Gian Song [2] and Ki Buem Kim [1,*]

[1] Hibrid Materials Center (HMC), Department of Nanotechnology and Advanced Materials Engineering, Sejong University, 209 Neungdong-ro, Gwangjin-gu, Seoul 05006, Korea; limgs78@hanmail.net (K.S.L.); ysgim82@gmail.com (Y.S.K.); shhong@sejong.ac.kr (S.H.H.)

[2] Division of Advanced Materials Engineering, Kongju National University, Cheonan, Chungnam 330-717, Korea; gasong@kongju.ac.kr

* Correspondence: kbkim@sejong.ac.kr

Received: 26 November 2019; Accepted: 28 December 2019; Published: 1 January 2020

Abstract: In this study, Mo–Si–N coatings were deposited on Si wafers and tungsten carbide substrates using a reactive direct current magnetron sputtering system with a MoSi powder target. The influence of sputtering parameters, such as the N_2 gas flow ratio and working pressure, on the microstructure and mechanical properties (hardness (H), elastic modulus (E), and H/E ratio) of the Mo–Si–N coatings was systematically investigated using X-ray diffractometry (XRD), scanning electron microscopy (SEM), nanoindentation, and transmission electron microscopy (TEM). The gas flow rate was a significant parameter for determining the crystallinity and microstructure of the coatings. A Mo_2N crystalline coating could be obtained by a high N_2 gas flow ratio of more than 35% in the gas mixture, whereas an amorphous coating could be formed by a low N_2 gas flow ratio of less than 25%. Furthermore, the working pressure played an important role in controlling the smooth surface and densified structure of the Mo–Si–N coating. For the amorphous Mo–Si–N coating deposited with the lowest working pressure (1 mTorr), the hardness, elastic modulus, and H/E ratio reached from 9.9 GPa, 158.8 GPa, and 0.062 up to 17.9 GPa, 216.1 GPa, and 0.083, respectively.

Keywords: Mo–Si–N; sputtering; amorphous coating; density; hardness

1. Introduction

Molybdenum nitride coatings have been found to have high hardness, excellent wear resistance, and a low friction coefficient compared with TiN and CrN coatings, which allows their use in various applications (i.e., hard coating, diffusion barrier, and tribological coating) [1–8]. Recently, ternary Mo–X–N (X = Al, Si, or C) coatings have been designed to further improve the mechanical properties of Mo–N-based coatings or to adjust the microstructure of the coating [3,9]. Especially, Mo–Si–N coatings deposited on a large content of Si have been studied for their nanocomposite structure, which consists of nanocrystalline Mo_2N embedded in amorphous matrixes (Si_3N_4) [3,10,11]. On the other hand, Mo–Si–N coatings deposited on a low content of Si have been rarely studied compared with nanocomposite coatings.

In particular, it was reported that the microstructure of Mo–Si–N coatings (for example, formation of crystalline or amorphous phases) is influenced by the composition and sputtering parameters [3,10,11]. The crystallization behavior of Mo–Si–N coatings is affected by the Si content and the N_2 gas flow ratio [12]. The N_2 gas flow ratio also plays an important role in controlling the microstructure, roughness, and crystallinity of the coating [13]. Furthermore, controlling the sputtering parameters, such as the working pressure, can improve the density of the coating structure and reduce the roughness of the

coating surface, and these parameters affect the mechanical properties of the coating [14]. According to Thornton's zone structure model [15], the density of a coating is substantially influenced by the working pressure and the substrate temperature during sputtering processes. A reduction of the working pressure enhances the mean free path of sputtered atoms and causes the coating to have a densified structure and a smooth surface [16]. Since Mo–Si–N amorphous coatings possess a lower friction coefficient than crystalline coatings [3], Mo–Si–N amorphous coatings are preferred as coating materials for cutting tools, which require a low friction coefficient. Nevertheless, the mechanical properties of Mo–Si–N amorphous coatings have not been studied in comparison with crystalline coatings [17].

In this study, Mo–Si–N coatings were fabricated using a reactive magnetron sputtering system at room temperature with a $Mo_{90}Si_{10}$ powder target. Our primary objective was the optimization of the sputtering conditions to achieve amorphous coatings. Specifically, the N_2 gas flow ratio and the working pressure were systemically adjusted to understand the effect of the gas flow ratio and working pressure on the microstructure, crystallinity, and mechanical properties of Mo–Si–N coatings. The microstructure and mechanical properties of Mo–Si–N coatings were investigated by X-ray diffractometry (XRD), field-emission scanning electron microscopy (FE-SEM), energy-dispersive X-ray spectroscopy (EDS), nanoindentation, and transmission electron microscopy (TEM).

2. Experimental

The Mo–Si–N coatings were deposited on p-type Si (100) wafers and WC (including Co 10%) substrates by a reactive high-vacuum direct current magnetron sputtering system (KVS-4006L, Korea Vacuum Tech, Gimpo-si, Korea). The $Mo_{90}Si_{10}$ target with a diameter of 101.6 mm and a thickness of 6.35 mm was made by mixing the metallic powders with high-purity molybdenum (99.8%) and silicon (99.8%), followed by a final cold-pressing (Plansee SE, Reutte, Austria). Prior to the deposition process, the Si wafers and WC substrates were ultrasonically cleaned and rinsed in acetone, ethanol, and distilled water for 5 min in each step. To fabricate coatings of homogeneous composition and thickness, the substrate stage was regularly rotated at 10 rpm. The chamber was evacuated below 5.0×10^{-6} Torr (6.6×10^{-4} Pa) and the sputtering gas was a mixture of high-purity argon (99.999%) and nitrogen (99.999%). Presputtering was performed under an input power of 300 W in Ar atmosphere for 10 min. No external heating was applied to the substrate during deposition. The microstructure, mechanical properties, and composition of the Mo–Si–N coatings were controlled by the N_2 gas flow ratio and the working pressure. First, the N_2 gas flow ratio ($R_N = N_2/(Ar + N_2)$) was tuned from 10% to 35% to optimize the condition for having an amorphous structure and high mechanical properties. Second, working pressures were controlled to form a high-density and smooth surface from 1 to 10 mTorr while retaining the N_2 gas flow ratio of 25%. The Mo–Si–N coatings were deposited for 90 min to produce coatings of micron-scale thickness. Typical deposition conditions for the Mo–Si–N coatings are summarized in Table 1.

Table 1. Deposition conditions of the Mo–Si–N coatings.

Process Parameter	Values (N_2 Gas Flow Ratio)	Values (Working Pressure)
Base pressure (Torr)	$<(5.0 \times 10^{-6})$	
Input power (W)	D.C 300	
N_2 gas flow ratio (%)	10, 15, 20, 25, 30, 35	25
Working pressure (mTorr)	10	10, 5, 2.5, 1
Deposition time (min)	90	
Rotation speed (rpm)	10	
Deposition temperature	Room temperature	

Structural analysis of the Mo–Si–N coatings was carried out using XRD (PANalytical/Empyrean/PC, Malvern, UK) with Cu $K_{\alpha 1}$ radiation (λ = 1.5406 Å) at a scanning rate of 2°/min. The microstructures of

the Mo–Si–N coatings (thickness and chemical composition) were examined using FE-SEM (SU-8010, Hitachi, Tokyo, Japan) equipped with EDS. The EDS measurements were conducted at least five times to ensure the reliability of the chemical composition. The deposition rate was calculated by dividing the thickness of the coating by the deposition time. The specimen preparation for TEM analysis was performed via focused ion beam thinning (FIB, Nova 600 NanoLab, FEI, Hillsboro, OR, USA). For detailed microstructural characterization, a TEM equipped with a Super-X EDS (TEM, Tecnai F20 G2, FEI, Hillsboro, OR, USA) was utilized. The hardness (H) and elastic modulus (E) of the coatings, which were derived from the Oliver–Pharr method [18], were measured using a nanoindenter (NHT-X, CSM, Needham, MA, USA) with a Berkovich diamond indenter tip at room temperature. To avoid substrate effects, the indentation measurements were conducted with a maximum indentation depth of less than ~1/10 of the film thickness [19,20]. The load–displacement curves were acquired from the depth control mode with loading and unloading rates of 10 mN/min. At least 15 measurements were performed for each sample to calculate average values by excluding the maximum and minimum values.

3. Results and Discussion

Figure 1a shows the X-ray diffraction patterns of the Mo–Si–N coatings deposited on silicon (100) wafers at various N_2 gas flow ratios from 10% to 35%. Because the thin coating thickness caused the inclusion of the structural information of the silicon wafer, the X-ray diffraction pattern of the silicon wafer was obtained to exclusively analyze the structure of the Mo–Si–N coatings. Under N_2 gas flow ratios from 10% to 30%, the Mo–Si–N coatings exhibited a broad halo pattern between 35° and 45° without significant evidence of crystallization, suggesting a typical amorphous structure. On the other hand, the X-ray diffraction pattern of the Mo–Si–N coating deposited by a N_2 gas flow ratio (R_N) of 35% displayed the crystalline Mo_2N phase with (111), (200), (220), and (311) orientations, respectively [3,21]. Figure 1b illustrates the chemical compositions of the Mo–Si–N coatings deposited on the WC substrates with N_2 gas flow ratios from 10% to 35% measured by SEM EDS. Every point indicates the average of five data points obtained from different regions on the coating. A WC substrate, instead of a silicon wafer, was selected as the substrate to avoid the possible inclusion of silicon coming from the substrate in the EDS measurements. When the N_2 gas flow ratio increased from 10% to 35%, the N content gradually increased from 19.1 at.% to 32.5 at.%. However, the Mo and Si contents were significantly decreased from 56.3 at.% to 42.5 at.% and 5.5 at.% to 4.3 at.% by the increase of N reactive gas, respectively. The increase of the N_2 gas flow ratio in the gas mixture led to a decrease of the Ar^+ ion intensity in plasma, causing a reduction in the sputtering yields of Mo and Si atoms [17]. In addition, the crystallinity of the Mo–Si–N coatings depended on the N_2 gas flow ratio and the Si content; specifically, a high N_2 gas flow ratio and low Si content improved the formation of crystalline MoN_X [12]. Kattelus et al. reported that the appearance of the first crystalline Mo_2N phase is consistent with the N composition value of 35 at.% [21]. The O content of the overall Mo–Si–N coatings was detected from 17.6 at.% to 20.6 at.%. The working pressure of 10 mTorr, our experimental condition, is a relatively high pressure. Coatings deposited at a high working pressure typically have a porous structure due to the short mean free path of the sputtered flux [14,22]. In addition, Tsai et al. explained that a large amount of O is probably incorporated into porous coatings when they are exposed to the atmosphere after deposition [14]. Therefore, it can be presumed that the Mo–Si–N coatings deposited at 10 mTorr had a porous structure and a large O content.

The surface SEM micrographs of the Mo–Si–N coatings deposited with N_2 gas flow ratios of 10%, 25%, and 35% are displayed in Figure 2a–c, respectively. There were cracks on the coating deposited at a N_2 gas flow ratio of 10% (Figure 2a). It was inferred that the cracks on the surface of the Mo–Si–N coating deposited by the N_2 gas flow ratio of 10% probably occurred due to the higher Ar gas ion content than that of the Mo–Si–N coating deposited at a N_2 gas flow ratio of 25%. It has been reported that the sputtering efficiency of Ar ions is higher than N ions [23,24]. Therefore, Ar gas ions accelerate the sputtered atoms to be faster than N gas ions, and the adatom sputtered by Ar gas ions arrives at the substrate with higher energy than the adatom sputtered by N gas ions. On the other hand, as the

N_2 gas flow ratio increased to 25%, the coating shown in Figure 2b had no cracks due to the reduction of the arrival rate of the sputtered species [25]. The coating in Figure 2c definitely shows coarse grains and a rough surface compared with those shown in Figure 2a,b. According to the XRD results, the coating shown in Figure 2c was crystalline Mo_2N, which had a different structure than the amorphous structure shown in Figure 2a,b.

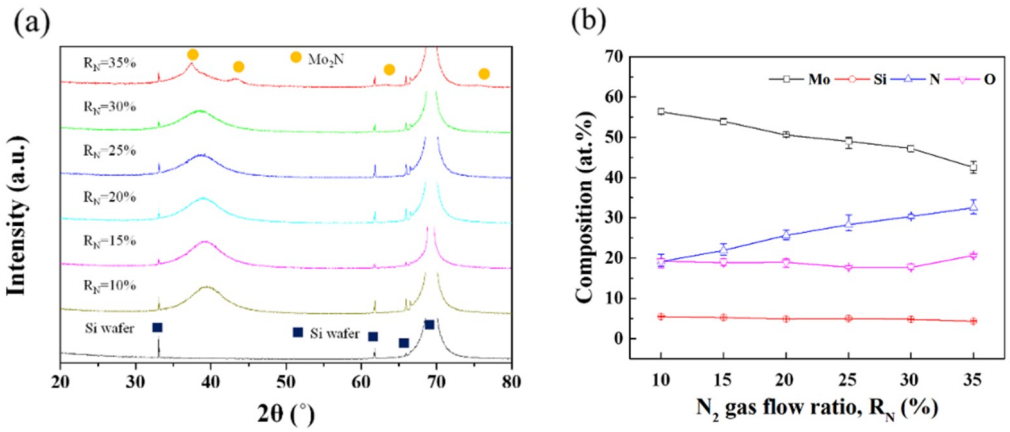

Figure 1. (**a**) X-ray diffractometry (XRD) patterns and (**b**) chemical composition of the Mo–Si–N coatings fabricated by diverse N_2 gas flow ratios from 10% to 35%, retaining the working pressure of 10 mTorr.

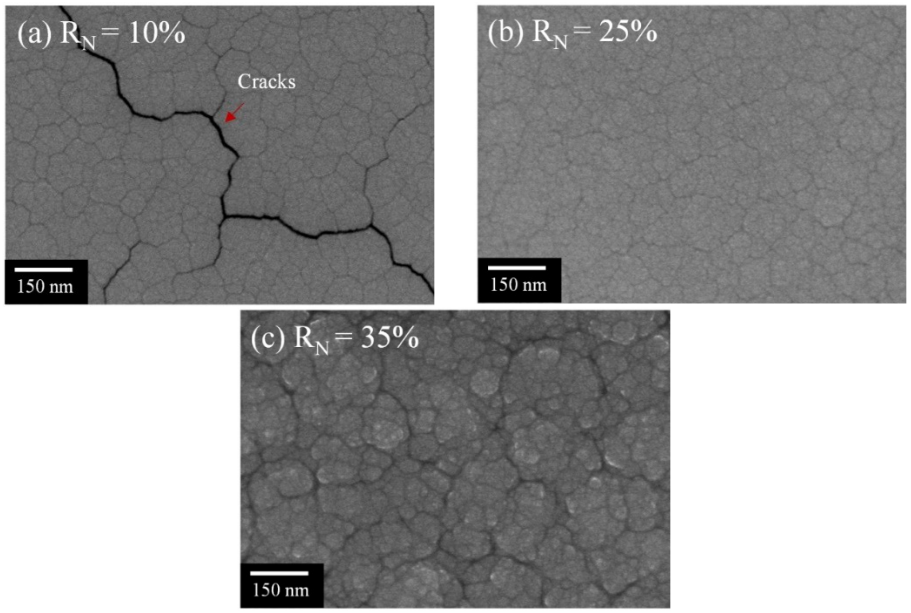

Figure 2. Surface field-emission scanning electron microscopy (FE-SEM) micrographs of the Mo–Si–N coatings deposited at N_2 gas flow ratios of (**a**) 10%, (**b**) 25%, and (**c**) 35%.

Figure 3 displays the deposition rate of the Mo–Si–N coatings fabricated under N_2 gas flow ratios from 10% to 35%. The deposition rate of Mo–Si–N coatings was calculated by dividing the thickness of the coating by the deposition time. As the N_2 gas flow ratio increased from 10% to 30%, the deposition rate of the Mo–Si–N coatings accordingly decreased from 22.8 nm/min for an R_N of 10% to 19.7 nm/min for an R_N of 30%. This phenomenon can be explained as follows: First, the target poisoning effect caused the reduction of the sputtering yields of Mo and Si during the sputtering process because excessive N_2 gas in the chamber formed the nitride on the surface of the metal target [13,26]. Second,

the sputtering efficiency of N_2 gas ions is typically lower than that of inert Ar gas ions [23,24]. However, the deposition rate of the Mo–Si–N coating deposited at a N_2 gas flow ratio of 35% slightly increased from 19.7 to 20.2 nm/min because of the formation of coarse grains (crystalline) and a rough surface.

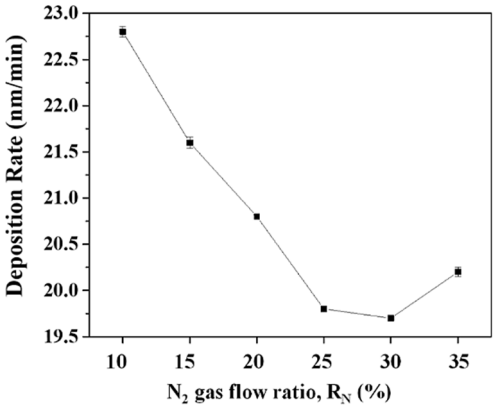

Figure 3. Deposition rate of the Mo–Si–N coatings deposited at various N_2 gas flow ratios from 10% to 35%, retaining the working pressure of 10 mTorr.

The hardness and elastic modulus of the Mo–Si–N coatings deposited with N_2 gas flow ratios from 10% to 35% are displayed in Table 2. The hardness increased from 7.4 ± 0.09 to 9.9 ± 0.23 GPa as the N_2 gas flow ratio increased from 10% to 25%, then decreased to 7.2 ± 0.14 GPa at a N_2 gas flow ratio of 35%. A similar trend was observed for the elastic modulus. The difference in the hardness between the amorphous coatings deposited under distinct sputtering conditions could have been caused by microstructural defects such as cracks, as shown in Figure 2a. The N_2 gas flow ratio of 10% led to cracks, which could have been produced by sputtered Mo and Si atoms with a higher kinetic energy due to a high Ar^+ ion intensity in plasma [13,17,27]. Therefore, the mechanical property results of the Mo–Si–N coating deposited at a N_2 gas flow ratio of 10% are not trustworthy due to the measurement of samples with cracks on the surface. However, the surface image of the coatings under a N_2 gas flow ratio of 25% (Figure 2b) showed no crack formation because of the low kinetic energy of the sputtered Mo and Si atoms. On the other hand, the decrease of the hardness from 25% to 35% is ascribed to the transition of the structure from amorphous to crystalline. Moreover, the coating deposited with a N_2 gas flow ratio of 35% (Figure 2c) had a rough surface and coarse grains, which caused the lower hardness compared with the fully amorphous structure [28]. *H*/*E* ratio values have recently been used to predict the plastic deformation and wear resistance of coatings [29–32]. The calculated *H*/*E* values of the Mo–Si–N coatings according to the N_2 gas flow ratios are indicated in Table 2. It was reported that a higher *H*/*E* value distributes the applied load to a wider region of the coating, which results in increased resistance to cracking and plastic deformation [29,31]. The values of the *H*/*E* ratio of the Mo–Si–N amorphous coatings produced with N_2 gas flow ratios from 15% to 25% were almost similar, except for the coatings deposited with R_N values of 10%, 30%, and 35%. However, the overall hardness and *H*/*E* ratio of the Mo–Si–N coatings were relatively lower compared with those of previous reports [11,33]. In this study, the O content of the Mo–Si–N coatings was around 20 at.%, which could be detrimental to the coating hardness [14,17]. A large amount of O in a coating means that the coating structure is porous because of the incorporation of O into the coating. Therefore, porous structures have low mechanical properties due to the low density and rough surface.

Table 2. Hardness (*H*), elastic modulus (*E*), and *H*/*E* ratios of the Mo–Si–N coatings deposited at N_2 gas flow ratios from 10% to 35%, retaining the working pressure of 10 mTorr.

N_2 Gas Flow Ratio (%)	Mechanical Properties		
	Hardness (GPa)	Elastic Modulus (GPa)	*H*/*E* Ratio
10	7.4 ± 0.09	149.0 ± 3.34	0.050 ± 0.0015
15	9.6 ± 0.14	156.5 ± 2.54	0.061 ± 0.0013
20	9.8 ± 0.11	157.7 ± 4.70	0.062 ± 0.0021
25	9.9 ± 0.23	158.8 ± 3.13	0.062 ± 0.0020
30	9.1 ± 0.17	156.4 ± 5.55	0.058 ± 0.0011
35	7.2 ± 0.14	145.3 ± 3.38	0.050 ± 0.0010

Figure 4a shows XRD patterns of Mo–Si–N coatings deposited on Si wafers with various working pressures. The XRD result measured from the Si wafer exclusively is also shown, since all the XRD patterns include the structural information of the Si wafer due to the thin thickness of the coatings. All the XRD patterns shown in Figure 4a exhibited a broad halo pattern between 35° and 45°, which is characteristic of a typical amorphous structure. No crystalline phases, such as Mo, Mo_3Si, Mo_5Si_3, $MoSi_2$, and Si_3N_4, were observed in the XRD results [3,11]. These results clearly indicate that Mo–Si–N amorphous coatings can be made on working pressures ranging from 1 to 10 mTorr. Figure 4b exhibits the chemical compositions of the Mo–Si–N amorphous coatings. As the working pressure decreased, the content of Mo and Si increased from 49.0 at.% to 65.3 at.% and 5.0 at.% to 6.4 at.%, respectively. However, the O content decreased from 17.1 at.% to 3.4 at.% as the working pressure decreased. As mentioned previously, coatings deposited at a high working pressure form a porous structure with a high probability of impurities being incorporated due to the short mean free path. On the other hand, coatings deposited at a low working pressure result in a dense structure and a smooth surface by the sputtered flux with a long mean free path, which reduces the probability of impurities being incorporated [14].

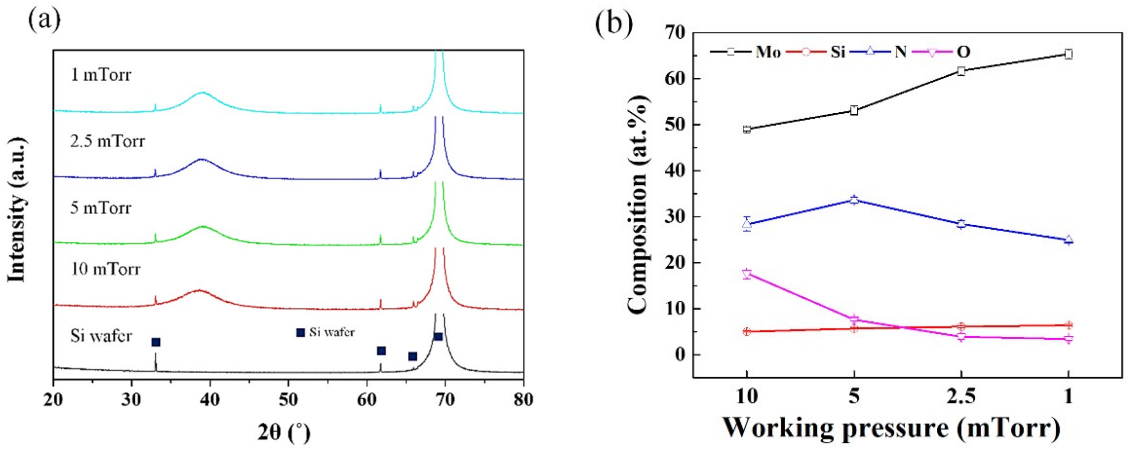

Figure 4. (**a**) XRD patterns and (**b**) energy-dispersive X-ray spectroscopy (EDS) results of the Mo–Si–N coatings produced under various working pressures of 10, 5, 2.5, and 1 mTorr, retaining the N_2 gas flow ratio of 25%.

The surface and cross-sectional SEM micrographs of the Mo–Si–N coatings deposited at various working pressures are illustrated in Figure 5. It can be seen that the thickness of the coatings gradually decreased from 1780 to 1380 nm due to the reduction of the working pressure from 10 to 1 mTorr. At a high working pressure, excessive gas in the chamber caused an increase in sputtering; thus, the sputter yields of Mo and Si increased. The surface and cross-sectional micrographs in Figure 5a,d show apparent microstructural changes in the Mo–Si–N coatings according to various working pressures.

The coatings deposited at high working pressures (10 and 5 mTorr) exhibited a rough and porous surface; however, a smooth and dense surface was obtained when deposition was at low working pressures (2.5 and 1 mTorr). Likewise, the cross-sectional images show the same result for the surface. At high working pressures, sputtered atoms obliquely colliding with gas species could arrive on the substrate and decrease the energy of bombardment on the coating, which is known as the shadowing effect [13]. Thus, the shadowing effect, caused by the higher working pressure, led to the formation of a porous structure between columns within the growing coatings [13,14,34]. In terms of the zone structure model [15], the microstructure in Figure 5d is close to the "Zone T structure", with dense and fibrous grains, while the microstructure in Figure 5a resembles the "Zone 1 structure", with porous and columnar grains. At a lower working pressure, the mobility of the adatoms was sufficient to induce atomic migration, allowing enough atomic rearrangement of adatoms [35]. This phenomenon has been described as the atomic peening effect, which increases the density and surface smoothness [35].

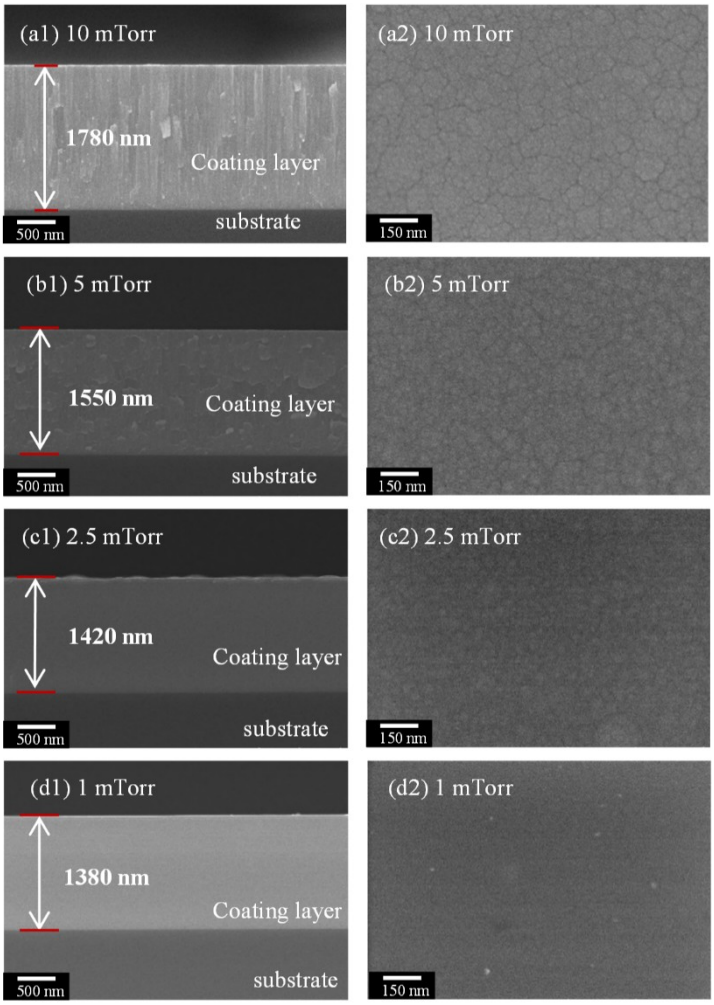

Figure 5. Cross-sectional and surface FE-SEM micrographs of the Mo–Si–N coatings deposited at various working pressures of (**a1**,**a2**) 10, (**b1**,**b2**) 5, (**c1**,**c2**) 2.5, and (**d1**,**d2**) 1 mTorr, retaining the N_2 gas flow ratio of 25%.

Figure 6a displays the cross-sectional bright-field (BF) TEM images and the selected area electron diffraction (SAED) pattern of the Mo–Si–N coating with the smoothest surface and highest density (1 mTorr). The thickness of the coating was measured to be 1480 nm, which is similar to that shown in Figure 5d. The SAED pattern indicated a hallow ring pattern, which demonstrated the formation of the homogenous amorphous structure throughout the deposited coating. Moreover, the coating deposited

with 1 mTorr clearly formed a densified structure without a columnar structure (Figure 6b). It can be seen that the high-resolution (HR) TEM image in Figure 6c exhibits randomly distributed adatoms without the regularities of lattice fringes in the coating, confirming the formation of the amorphous structure [36]. The fast Fourier transform (FFT) diffractogram inserted in Figure 6(c1) shows a hollow ring pattern with the same result as the SAED pattern.

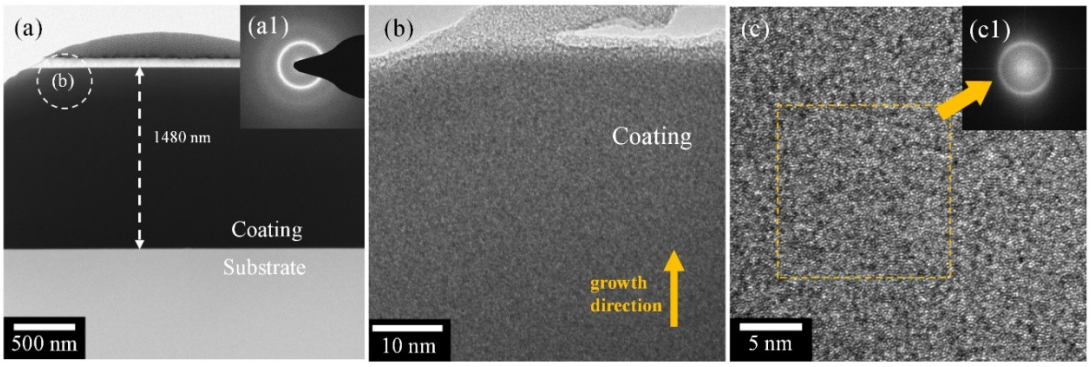

Figure 6. (**a**,**b**) Bright-field (BF) ((**a1**) inserted selected area electron diffraction (SAED) pattern) and (**c**) high-resolution (HR) ((**c1**) inserted FFT diffractogram) transmission electron microscopy (TEM) images of the Mo–Si–N coating deposited at a N_2 gas flow ratio of 25% and a working pressure of 1 mTorr.

The hardness, elastic modulus, and *H*/*E* ratio values of the Mo–Si–N coatings deposited on Si wafers at diverse working pressures from 10 to 1 mTorr are indicated in Table 3. With a working pressure of 10 mTorr, the hardness and elastic modulus were measured to be 9.9 ± 0.23 and 158.8 ± 3.13 GPa, respectively. The reduced working pressure (1 mTorr) resulted in an increase of the hardness and elastic modulus up to 17.9 ± 0.19 and 216.1 ± 2.90 GPa, respectively. The H/E values of Mo–Si–N coatings with 10, 5, 2.5, and 1 mTorr were 0.062 ± 0.0020, 0.065 ± 0.0022, 0.082 ± 0.0014, and 0.083 ± 0.0017, respectively. Despite having the same amorphous structure, the mechanical properties of the Mo–Si–N coating were enhanced by about 2-fold due to the transformation from a rough to a smooth surface and from a porous to a densified structure as the working pressure decreased step by step. Also, these coating structure transformations caused a reduction of oxygen incorporation, as indicated in the EDS and SEM results [13].

Table 3. Hardness, elastic modulus, and *H*/*E* of the Mo–Si–N coatings deposited at working pressures of 10, 5, 2.5, and 1 mTorr, retaining a N_2 gas flow ratio of 25%.

Working Pressure (mTorr)	Mechanical Properties		
	Hardness (GPa)	Elastic Modulus (GPa)	*H*/*E* Ratio
10	9.9 ± 0.23	158.8 ± 3.13	0.062 ± 0.0020
5	12.7 ± 0.17	194.1 ± 5.20	0.065 ± 0.0022
2.5	16.9 ± 0.29	208.0 ± 2.18	0.082 ± 0.0014
1	17.9 ± 0.19	216.1 ± 2.90	0.083 ± 0.0017

Based on the present microstructural characterization and mechanical tests, the mechanical properties of the Mo–Si–N coatings were found to be strongly dependent upon the coating structures, such as crystalline and amorphous structures. Specifically, the amorphous Mo–Si–N coatings exhibited better mechanical properties than the coating including a partial crystalline structure. The formation of the amorphous coating and its mechanical properties can be controlled by the gas flow ratio and working pressures. First, the gas flow ratio is a crucial process parameter when forming an amorphous coating structure. Especially, a N_2 gas flow ratio of 25% is required for the formation of the amorphous phase without cracking and a partial crystalline phase in the coating layer. Secondly, the working pressure plays an important role in controlling the mechanical properties of the amorphous coatings.

The reduction of the working pressure increases the coating density and reduces oxygen incorporation and roughness. Therefore, it is believed that these two processing parameters should be considered when forming an amorphous coating and improving the mechanical properties [20].

4. Conclusions

Mo–Si–N coatings were deposited by adjusting the N_2 gas flow ratios from 10% to 35% at room temperature using a reactive magnetron sputtering system. It was found that microstructures of the Mo–Si–N coatings at N_2 gas flow ratios from 10% to 25% consisted of an amorphous structure. At the N_2 gas flow ratios of 30% and 35%, however, the Mo–Si–N coatings formed a partial Mo_2N crystalline phase. The Mo–Si–N coating with a N_2 gas flow ratio of 25% showed superior mechanical properties, a hardness of 9.9 GPa, an elastic modulus of 158.8 GPa, and an H/E ratio of 0.062. To enhance the density of the coatings and reduce the probability of impurities being incorporated while maintaining an amorphous structure, the Mo–Si–N coatings were fabricated by controlling working pressures from 1 to 10 mTorr at a N_2 gas flow ratio of 25% at room temperature. All the Mo–Si–N coatings under working pressures from 1 to 10 mTorr showed an amorphous structure. The decrease in the working pressure resulted in an increased coating density and a reduced O content from 19.1 at.% to 3.4 at.%. When the working pressure decreased from 10 to 1 mTorr, the hardness, elastic modulus, and H/E values increased up to 17.9 GPa, 216.1 GPa, and 0.083, respectively.

Author Contributions: Conceptualization, K.S.L. and K.B.K.; methodology, K.S.L.; validation, S.H.H. and G.S.; formal analysis, K.S.L. and Y.S.K.; investigation, K.S.L.; data curation, Y.S.K.; writing—original draft preparation, K.S.L.; writing—review and editing, S.H.H. and G.S.; supervision, K.B.K.; funding acquisition, K.B.K. All authors have read and agreed to the published version of the manuscript.

Funding: This work was supported by the Technology Innovation Program (Project No. 10063052, Development of advanced nano-micron coating material and coated cutting tool for Hard-to-Cut), funded by the Ministry of Trade, Industry, and Energy (MOTIE, Korea); the Human Resources Development of the Korea Institute of Energy Technology Evaluation and Planning (KETEP) grant, funded by the Korean Government Ministry of Trade, Industry, and Energy (No. 20164030201340); and the National Research Foundation of Korea (NRF) grant, funded by the Korean Government (MSIT) (No. 2018R1A2B3007167); the Ministry of Trade, Industry and Energy (MOTIE) and Korea Institute for Advancement of Technology (KIAT) through the International Cooperative R&D program. (Project No. P0011878).

Conflicts of Interest: The authors declare no conflict of interest.

References

1. Hones, P.; Martin, N.; Regula, M.; Lévy, F. Structural and mechanical properties of chromium nitride, molybdenum nitride, and tungsten nitride thin films. *J. Phys. D: Appl. Phys.* **2003**, *36*, 1023. [CrossRef]
2. Kazmanli, M.; Ürgen, M.; Cakir, A. Effect of nitrogen pressure, bias voltage and substrate temperature on the phase structure of Mo–N coatings produced by cathodic arc PVD. *Surf. Coat. Technol.* **2003**, *167*, 77–82. [CrossRef]
3. Heo, S.J.; Kim, K.H.; Kang, M.C.; Suh, J.H.; Park, C.-G. Syntheses and mechanical properties of Mo–Si–N coatings by a hybrid coating system. *Sur. Coat. Technol.* **2006**, *201*, 4180–4184. [CrossRef]
4. Wang, Y.; Lin, R.Y. Amorphous molybdenum nitride thin films prepared by reactive sputter deposition. *Mater. Sci. Eng. B.* **2004**, *112*, 42–49. [CrossRef]
5. Öztürk, A.; Ezirmik, K.; Kazmanlı, K.; Ürgen, M.; Eryılmaz, O.; Erdemir, A. Comparative tribological behaviors of TiN, CrN and MoN Cu nanocomposite coatings. *Tribol. Int.* **2008**, *41*, 49–59. [CrossRef]
6. Xiang, J.; Lin, Z.; Renoux, E.; Wu, F. Microstructure evolution and indentation cracking behavior of MoN multilayer films. *Surf. Coat. Technol.* **2018**, *350*, 1020–1027. [CrossRef]
7. Ürgen, M.; Eryilmaz, O.; Çakir, A.; Kayali, E.; Nilüfer, B.; Işik, Y. Characterization of molybdenum nitride coatings produced by arc-PVD technique. *Surf. Coat. Technol.* **1997**, *94*, 501–506. [CrossRef]
8. Chuang, J.-C.; Tu, S.-L.; Chen, M.-C. Sputter-deposited Mo and reactively sputter-deposited Mo–N films as barrier layers against Cu diffusion. *Thin Solid Films* **1999**, *346*, 299–306. [CrossRef]
9. Nicolet, M.-A.; Giauque, P. Highly metastable amorphous or near-amorphous ternary films (mictamict alloys). *Microelectron. Eng.* **2001**, *55*, 357–367. [CrossRef]

10. Hirvonen, J.-P.; Suni, I.; Kattelus, H.; Lappalainen, R.; Torri, P.; Kung, H.; Jervis, T.; Nastasi, M.; Tesmer, J. Crystallization and oxidation behavior of Mo–Si–N coatings. *Surf. Coat. Technol.* **1995**, *74*, 981–985. [CrossRef]
11. Liu, Q.; Fang, Q.; Liang, F.; Wang, J.; Yang, J.; Li, C. Synthesis and properties of nanocomposite MoSiN hard films. *Surf. Coat. Technol.* **2006**, *201*, 1894–1898. [CrossRef]
12. Musil, J.; Dohnal, P.; Zeman, P. Physical properties and high-temperature oxidation resistance of sputtered Si_3N_4/MoN_x nanocomposite coatings. *J. Vac. Sci. Technol. B.* **2005**, *23*, 1568–1575. [CrossRef]
13. Tsai, D.-C.; Huang, Y.-L.; Lin, S.-R.; Liang, S.-C.; Shieu, F.-S. Effect of nitrogen flow ratios on the structure and mechanical properties of (TiVCrZrY)N coatings prepared by reactive magnetron sputtering. *Appl. Surf. Sci.* **2010**, *257*, 1361–1367. [CrossRef]
14. Tsai, D.-C.; Chang, Z.-C.; Kuo, B.-H.; Chen, B.-C.; Chen, E.-C.; Shieu, F.-S. Wide variation in the structure and physical properties of reactively sputtered (TiZrHf)N coatings under different working pressures. *J. Alloy. Compd.* **2018**, *750*, 350–359. [CrossRef]
15. Thornton, J.A. Influence of apparatus geometry and deposition conditions on the structure and topography of thick sputtered coatings. *J. Vac. Sci. Technol.* **1974**, *11*, 666–670. [CrossRef]
16. Xu, Y.; Cui, J.; Cui, H.; Zhou, H.; Yang, Z.; Du, J. Influence of deposition pressure, substrate temperature and substrate outgassing on sorption properties of Zr–Co–Ce getter films. *J. Alloy. Compd.* **2016**, *661*, 396–401. [CrossRef]
17. Xiang, J.-Y.; Wu, F.-B. Gas inlet and input power modulated sputtering molybdenum nitride thin films. *Surf. Coat. Technol.* **2017**, *332*, 161–167. [CrossRef]
18. Yan, W.; Pun, C.L.; Simon, G.P. Conditions of applying Oliver–Pharr method to the nanoindentation of particles in composites. *Compos. Sci. Technol.* **2012**, *72*, 1147–1152. [CrossRef]
19. Bull, S. Nanoindentation of coatings. *J. Phys. D: Appl. Phys.* **2005**, *38*, R393. [CrossRef]
20. Kim, Y.S.; Park, H.J.; Mun, S.C.; Jumaev, E.; Hong, S.H.; Song, G.; Kim, J.T.; Park, Y.K.; Kim, K.S.; Jeong, S.I. Investigation of structure and mechanical properties of TiZrHfNiCuCo high entropy alloy thin films synthesized by magnetron sputtering. *J. Alloy. Compd.* **2019**, *797*, 834–841. [CrossRef]
21. Kattelus, H.; Koskenala, J.; Nurmela, A.; Niskanen, A. Stress control of sputter-deposited Mo–N films for micromechanical applications. *Microelectronic Eng.* **2002**, *60*, 97–105. [CrossRef]
22. French, B.; Bilello, J. In situ observations of the real-time stress-evolution and delamination of thin Ta films on Si (100). *Thin Solid Films* **2004**, *446*, 91–98. [CrossRef]
23. Mason, R.S.; Pichilingi, M. Sputtering in a glow discharge ion source-pressure dependence: theory and experiment. *J. Phys. D: Appl. Phys.* **1994**, *27*, 2363. [CrossRef]
24. Tsau, C.-H.; Chang, Y.-H. Microstructures and mechanical properties of $TiCrZrNbN_x$ alloy nitride thin films. *Entropy* **2013**, *15*, 5012–5021. [CrossRef]
25. Shi, Y.; Pan, F.; Bao, M.; Yang, Z.; Wang, L. Effect of N_2 flow rate on structure and property of $ZrNbAlN_x$ multilayer films deposited by magnetron sputtering. *J. Alloy. Compd.* **2013**, *559*, 196–202. [CrossRef]
26. Anitha, V.; Major, S.; Chandrashekharam, D.; Bhatnagar, M. Deposition of molybdenum nitride thin films by rf reactive magnetron sputtering. *Surf. Coat. Technol.* **1996**, *79*, 50–54. [CrossRef]
27. Liu, L.; Zhu, J.; Hou, C.; Li, J.; Jiang, Q. Dense and smooth amorphous films of multicomponent FeCoNiCuVZrAl high-entropy alloy deposited by direct current magnetron sputtering. *Mater. Design.* **2013**, *46*, 675–679. [CrossRef]
28. Hsueh, H.-T.; Shen, W.-J.; Tsai, M.-H.; Yeh, J.-W. Effect of nitrogen content and substrate bias on mechanical and corrosion properties of high-entropy films $(AlCrSiTiZr)_{100-x}N_x$. *Surf. Coat. Technol.* **2012**, *206*, 4106–4112. [CrossRef]
29. Musil, J.; Kunc, F.; Zeman, H.; Polakova, H. Relationships between hardness, Young's modulus and elastic recovery in hard nanocomposite coatings. *Surf. Coat. Technol.* **2002**, *154*, 304–313. [CrossRef]
30. Leyland, A.; Matthews, A. On the significance of the *H/E* ratio in wear control: a nanocomposite coating approach to optimised tribological behaviour. *Wear* **2000**, *246*, 1–11. [CrossRef]
31. Musil, J. Hard nanocomposite coatings: Thermal stability, oxidation resistance and toughness. *Surf. Coat. Technol.* **2012**, *207*, 50–65. [CrossRef]
32. Qi, Z.; Wu, Z.; Zhang, D.; Wei, B.; Wang, J.; Wang, Z. Effect of sputtering power on the chemical composition, microstructure and mechanical properties of CrN_x hard coatings deposited by reactive magnetron sputtering. *Vacuum* **2017**, *145*, 136–143. [CrossRef]

33. Blinkov, I.; Chernogor, A.; Volkhonskii, A.; Sergevnin, V.; Belov, D.; Sargaeva, O. Phase composition, structure, and mechanical properties of arc PVD Mo–Si–Al and Mo–Si–Al–N coatings. *Inorg. Mater.* **2017**, *53*, 125–134. [CrossRef]
34. Moon, Y.-K.; Bang, B.; Kim, S.-H.; Jeong, C.-O.; Park, J.-W. Effects of working pressure on the electrical and optical properties of aluminum-doped zinc oxide thin films. *J. Mater. Sci. Mater. Electron.* **2008**, *19*, 528–532. [CrossRef]
35. Clemens, B. Effect of sputtering pressure on the structure and solid-state reaction of titanium-nickel compositionally modulated film. *J. Appl. Phys.* **1987**, *61*, 4525–4529. [CrossRef]
36. Kim, K.; Das, J.; Venkataraman, S.; Yi, S.; Eckert, J. Work hardening ability of ductile $Ti_{45}Cu_{40}Ni_{7.5}Zr_5Sn_{2.5}$ and $Cu_{47.5}Zr_{47.5}Al_5$ bulk metallic glasses. *Appl. Phys. Lett.* **2006**, *89*, 071908. [CrossRef]